Check for updates

View Article Online
View Journal | View Issue

Green approach for the fabrication of a ternary nanocatalyst (Ag-ZnONPs@Cy) for visible light-induced photocatalytic reduction of nitroarenes to aminoarenes†

Dana A. Kader [ID] *[ab]

In recent times, the incorporation of metal oxide nanoparticles with organic dyes has piqued the interest of numerous researchers due to their diverse applications under visible light instead of UV radiation. This investigation employed a three-step methodology to fabricate cyanidin-sensitized silver-doped zinc oxide nanoparticles (Ag-ZnO@Cy). Initially, cyanidin dye was extracted from fresh black mulberry fruit, followed by the eco-friendly synthesis of Ag-ZnO nanoparticles (Ag-ZnONPs). The successful integration of the prepared cyanidin dye with Ag-ZnONPs was achieved through a straightforward, environmentally benign, and cost-efficient procedure. The resultant ternary composite underwent comprehensive characterization and confirmation utilizing various techniques, such as SEM, FT-IR, EDX, DRS, elemental mapping, and XRD. The experimental results for Ag-ZnONPs@Cy demonstrated that the nanocrystalline wurtzite exhibited spherical shapes with an average crystal size of 27.42 nm. Moreover, the photocatalytic activity of the synthesized Ag-ZnONPs@Cy was meticulously investigated under blue LED light irradiation. This inquiry encompassed examinations of catalyst amount, regeneration, stability, reusability, and the influence of light source on the hydrogenation of nitroarenes to the corresponding aminoarenes. The findings shed light on the potential of this composite for diverse photocatalytic applications.

1. Introduction

Over the past few years, organic dyes have played a crucial role in advancing the application of metal oxide nanoparticles. These nanoparticles have found diverse uses, such as acting as efficient photocatalysts for the removal of organic pollutants,[1] contributing to the design of more efficient solar cells,[2] facilitating dye degradation processes,[3] enabling hydrogen production,[4] and promoting various organic transformations.[5] The realm of semiconductor photocatalysis, a subset of photochemistry, has attracted considerable interest owing to its optimistic capacity for producing valuable chemicals. This distinct method leverages the potency of light as an economical energy resource, facilitating the transformation of demanding reaction conditions into gentler and eco-friendlier alternatives. As a result, researchers have been increasingly focusing their efforts on developing photochemical reactions that can be initiated under visible light, aligning with the principles of green chemistry and sustainable practices. This pursuit aims to reduce the reliance on conventional energy-intensive processes and pave the way for more sustainable and eco-friendly chemical transformations.[3,6]

A wide array of metal oxide nanoparticles, including MnO, CdS, TiO$_2$, MgO, ZnO, and WO$_3$, have been extensively utilized as photocatalytic materials in organic transformations. The reason behind their widespread adoption lies in their exceptional attributes, such as remarkable chemical stability, potent catalytic capabilities, low toxicity, and cost-effectiveness. As a result, these materials are highly sought after for promoting a diverse range of organic reactions through photocatalysis.[7–15]

Zinc oxide nanoparticles (ZnONPs) have established their versatility as an oxide material, finding extensive applications across diverse domains. These include uses in sunscreens and cosmetics,[16] antibacterial coatings,[17] electronics and optoelectronics,[18] textiles,[19] nanomedicine,[20] anti-corrosion coatings,[21] gas sensors,[22] transparent conductive films,[23] piezoelectric devices,[24] and photocatalysis.[25,26] Although there are several advantages to using ZnONPs as a photocatalyst, they also come with certain drawbacks.[27] The most significant drawback is that ZnONPs can only participate in photochemical reactions when activated by UV light. Unfortunately, UV light is not an abundant source of radiation, and both green sources of light and

[a]Department of Chemistry, College of Education, University of Sulaimani, Old Campus, Kurdistan Region, 46001, Iraq. E-mail: dana.kader@univsul.edu.iq

[b]Pharmacy Department, Komar University of Science and Technology, Kurdistan Region, Sulaimani 46001, Iraq

sunlight typically contain only 5–8% of UV,[28] which limits the efficiency of ZnONPs in these conditions. The effectiveness of photocatalysis relies heavily on two key factors related to ZnO nanostructures. First, it depends on how much of the solar spectrum these nanostructures can capture. Efficient utilization of a broader range of wavelengths ensures better overall performance. Second, the life-time of the formed electron–hole pair during the photocatalytic process plays a crucial role. The longer the pair remains separated without recombination, the higher the photocatalytic efficiency achieved.

A three-pronged strategy can be embraced to heighten the efficiency of zinc oxide nanoparticles, which encounter constraints due to their wide band-gap. Firstly, the absorption of sunlight can be elongated to engender a larger number of electron–hole pairs. Secondly, the photons-to-electrons conversion can be fine-tuned to augment proficiency further. Lastly, prolonging the photo-generated electron–hole lifespan pairs can sustain their activity for an extended period.[29–38] Overcoming these challenges demands the implementation of modifications involving an assortment of additives, such as organic dyes, metal complexes, and metal or non-metal ions. These adjustments present a promising resolution to address the aforementioned limitations.[39]

Photosensitization involves a process where a photosensitizer is adsorbed onto the surface of a semiconductor. This photosensitizer absorbs light energy and then converts it into chemical energy. Under favorable conditions, this energy is transferred to typically unreactive substrates through photochemical reactions. Among the most extensively studied visible light photosensitizers are diverse organic dyes like riboflavin, Eosin-Y, alizarin red S, rose bengal, inorganic sensitizers, and inorganic metal complexes. When a sensitizer absorbs light, it becomes excited and injects an electron into the conduction band of the semiconductor.[40]

The hydrogenation of nitro aromatics to produce corresponding amines is a crucial organic transformation widely employed in industries, serving as a starting material for synthesizing a diverse array of organic compounds. However, traditional reduction methods involve using environmentally hazardous chemicals and often lead to undesirable toxic metal sludge generation. Fortunately, advancements have been made in recent times towards greener methodologies for reducing nitroarenes, particularly under visible light conditions. These greener approaches aim to minimize the environmental impact while achieving efficient and sustainable transformations.

This study synthesized a ternary visible light-responsive hybrid catalyst, cyaniding dye-sensitized silver doped zinc oxide nanoparticles denoted as Ag-ZnONPs@Cy, using an entirely green approach. The sensitizer, cyanidin dye, was extracted from fresh black mulberry fruit and utilized to activate pre-fabricated Ag-ZnONPs. The resulting ternary composite was employed to hydrogenate nitroarenes to form the corresponding aminoarenes but with a notable distinction. Instead of using UV light, the catalytic reactions were carried out under blue light irradiation. This innovative approach not only enhances the photocatalytic activity but also underscores the eco-friendly nature of the overall process.

2. Experimental part

2.1. Chemicals, materials, and characterization methodology

All chemical compounds and solvents obtained from Sigma-Aldrich were of analytical quality and utilized as received without additional purification steps. Zinc chloride (CAS#: 7646-85-7, ≥98%, molecular weight: 136.30 g mol^{-1}), silver nitrate (CAS#: 7761-88-8, ≥99%, molecular weight: 168.87 g mol^{-1}), acetonitrile (CAS#: 75-05-8, ≥99.9%, molecular weight: 41.05 g mol^{-1}), acetone (CAS#: 67-64-1, ≥99.5%, molecular weight: 58.08 g mol^{-1}), ethanol (CAS#: 64-17-5, 95%, molecular weight: 46.07 g mol^{-1}) nitroarenes (CAS#: 98-95-3, 586-78-7, 41085-43-2, 7149-70-4, 100-17-4, 100-02-7, 619-72-7, 5401-94-5, 613-50-3, 22280-56-4, 16013-85-7, 38533-61-8). 5 W LED strip lights were employed for irradiation, consisting of a red lamp, a green lamp, a blue lamp, and a white light. The ^{1}H-NMR and ^{13}C-NMR spectra were recorded using a 400 MHz Bruker Avance DRX spectrometer (Billerica, MA, USA). The PerkinElmer spectrophotometer and FT-IR spectra were acquired (Waltham, MA, USA). For structural analysis, an X-ray diffractometer (PANalytical X'PERT-PRO MRD) equipped with a Cu Kα ($\lambda = 0.15406$ nm) radiation source was used to scan between 10° and 80° at a rate of 2° min^{-1}. The absorption spectrum was analyzed using a UV–vis diffuse reflectance spectrophotometer (UV-Vis-DRS, SCINCO Model S-4100). For Nanostructural and chemical analyses of the fabricated catalysts, scanning electron microscopy (LV-SEM, JSM-6380LV; JEOL; Sollentuna, Sweden) and energy-dispersive X-ray spectroscopy (EDX, INCAx-sight; Oxford Instruments; Abingdon, United Kingdom) techniques were employed.

2.2. Preparation of neem leaf extract

In Sulaimani, Iraq, a batch of fifteen grams of freshly harvested Neem leaves underwent a rigorous washing procedure with distilled water to ensure the removal of any impurities. Following this thorough washing, the leaves were finely chopped and combined with 100 mL of distilled water. The mixture was then heated for approximately one hour at a temperature of 60 °C. After the heating process, the extracts were allowed to cool down before being filtrated using Whatman filter paper. Finally, the filtered extracts were stored and fully prepared for future use.

2.3. Procedure for fabrication of Ag-ZnONPs

Silver-doped zinc oxide nanoparticles (Ag-ZnONPs) were produced by combining 45 millimoles of ZnCl$_2$ and 5 millimoles of AgNO$_3$ in a beaker containing 50 milliliters of distilled water (DW) under continuous stirring. The stirring persisted until a clear solution emerged, indicating the complete dissolution of the initial substances. Gradually, the neem leaf extract, previously prepared (100 mL), was added drop by drop from a burette into the stirred solution, maintaining the stirring for approximately 45 minutes. Afterwards, the resulting precipitate settled overnight and was subsequently separated through decantation. The separated precipitate underwent a sequential

washing process involving acetone, ethanol, and water. The pure precipitate was then obtained through centrifugation at 4500 rpm for 10 minutes. To achieve Ag-doped ZnONPs in dry powder form, the previously obtained precipitate was placed in an oven at 75 °C for 4 hours. Following this, the material underwent calcination at 300 °C for 2.5 hours.

2.4. Procedure for fabrication of Ag-ZnONPs@Cy

A novel ternary composite (Ag-ZnONPs@Cy) was synthesized through a straightforward, green, and cost-effective process. The procedure involved the following steps: To begin, 25 grams of freshly collected black mulberry fruit were carefully washed with water to eliminate any dust or impurities. Subsequently, the black mulberries were placed onto a piece of cotton fabric (cheesecloth) and pressed until all the fruit juice was extracted. Following the successful extraction of the cyanidin dye, the resulting black-violet mulberry juice was combined with 25 mL of distilled water. The mixture was then filtered to eliminate impurities, and the extract was subsequently evaporated and dried in an oven at 75 °C to obtain the powdered form of the cyanidin dye. Subsequently, a 1000 ppm (1 g in 1 L) solution of the dye was prepared. For the adsorption process, 250 mL of this dye solution was taken, and 2 grams of pre-fabricated Ag-ZnONPs were introduced. The mixture was subjected to boiling for 30 minutes. The successful combination of the cyanidin dye from the black mulberry and the silver-doped zinc oxide nanoparticles was confirmed by the change in particle color from white to reddish brown. Following this, the synthesized Ag-ZnONPs@Cy composite was separated using a centrifuge at 4500 rpm for 15 minutes. It was subsequently washed three times with 10 mL of distilled water in each wash. Additional washing steps were carried out using ethanol and acetone to ensure the removal of any remaining impurities. Finally, the composite was dried at 100 °C for 4 hours to obtain the desired product.

2.5. Photocatalytic activity: reduction of nitroarenes

The photocatalytic reduction of nitroarenes in the presence of triethanolamine (TEOA) was carried out under blue light irradiation ($\lambda > 425$ nm). To initiate the reaction, a fixed amount of catalyst (10 mg) was added to a mixture of 15 mL acetonitrile solution containing 1 mmol (1 equiv.) of nitroarenes and 10 equiv. of TEOA in a test tube. Before commencing the reaction, N_2 gas was bubbled into the solution for 45 minutes, and then the reaction vessel was sealed. The reaction was performed under steady stirring (500 rpm), with the reaction mixture exposed to visible light ($\lambda > 425$ nm) using a 5 W LEDs light placed 5 cm away from the reaction vessel at room temperature. The progress of the reactions was monitored using UV-vis spectroscopy. Following the completion of the reaction, the photocatalyst was recovered by subjecting the mixture to centrifugation at 5000 rpm for 15 minutes. The solvent was evaporated under reduced pressure, and the resulting product was isolated using silica-gel column chromatography with hexane-ethyl acetate as the eluent. The product yield percentage was determined using the following formula:

$$\text{Yield (\%)} = [\text{actual yield (mg)/theoretical yield (mg)}] \times 100$$

The purity and identity of the resulting products (1b–12b) were analyzed using ^{1}H-NMR and ^{13}C-NMR techniques. An illustrative representation of the complete fabrication and application process of Ag-ZnONPs@Cy in Scheme 1.

3. Results and discussion

3.1. Fabrication of Ag-ZnONPs@Cy

The ternary nanocatalyst was synthesized through a three-step process. Firstly, fresh black mulberry fruit was locally sourced, and its cyanidin dye juice was extracted. Secondly, Ag-ZnONPs were synthesized through an eco-friendly and uncomplicated approach employing neem leaf extract. This extract aids in converting the chemical salt into nanoparticles while also serving as a capping agent during the reduction process.[41] Lastly, the Ag-ZnONPs@Cy composite was synthesized through a simple procedure, and further details can be found in the experimental section. Various methods such as DRS, SEM, elemental mapping, XRD, FT-IR, EDX, and UV-visible spectroscopy were employed to characterize the photocatalyst comprehensively. These techniques provided insights into the structural and chemical properties of the nanocatalyst.

3.2. Complexation strategy between ZnONPs and cyanidin (Cy) dye

Cyanidin dye, possessing multiple hydroxyl groups, can bind to the surface of zinc oxide nanoparticles through chelation or bridging, releasing water molecules (dehydration), as depicted in Fig. 1. The high electron affinity of zinc compared to titanium makes zinc more prone to exhibit a stronger interaction with ligands.[42] The formation of surface complexes occurs between ZnO and the phenolic hydroxyl groups of cyanidin, akin to the observed interactions reported with other phenolic compounds.[42–45]

The quantity of cyanidin dye in the ternary nano catalyst was determined as follow:

After the adsorption process, the residual dye was separated from Ag-ZnONPs@Cy through centrifugation. The concentration of the dye was determined using UV-Vis spectroscopy at the lambda max (530 nm) of the cyanidin dye. Following the calculation, the concentration was found to be 723 ppm. The amount of adsorbed dye (in milligrams) on the surface of Ag-ZnONPs was then computed using the following equation:

$$\text{Adsorbed cyanidin dye (mg g}^{-1}) = (C_0 - C_e) \times V/m$$

C_0 is the initial concentration of the dye solution (ppm). C_e is the final concentration of the dye solution after adsorption (ppm). V is the volume of the dye solution (L). m is the mass of the metal oxide (g).

The determined amount was found to be 34.625 mg g^{-1} of cyanidin on Ag-ZnONPs.

Scheme 1 Illustrative process for producing and utilizing Ag-ZnONPs@Cy, depicted step-by-step.

3.3. Characterizations

3.3.1. SEM, EDX and elemental mapping. Fig. 2 and 3 illustrate the scanning electron microscopy (SEM), energy-dispersive X-ray spectroscopy (EDX), and elemental mapping images of the synthesized Ag-ZnONPs and Ag-ZnONPs@Cy. This analysis aimed to assess the structural and elemental characteristics of the synthesized Ag-ZnONPs and Ag-ZnONPs@Cy. The investigations were carried out at magnifications of 200 nm and 1 μm. Fig. 2a and b show that the Ag-ZnONPs possess a spherical structure and are arranged in a regular pattern, displaying particle sizes ranging from 20 to 50 nm. Although there are instances of particle agglomeration,
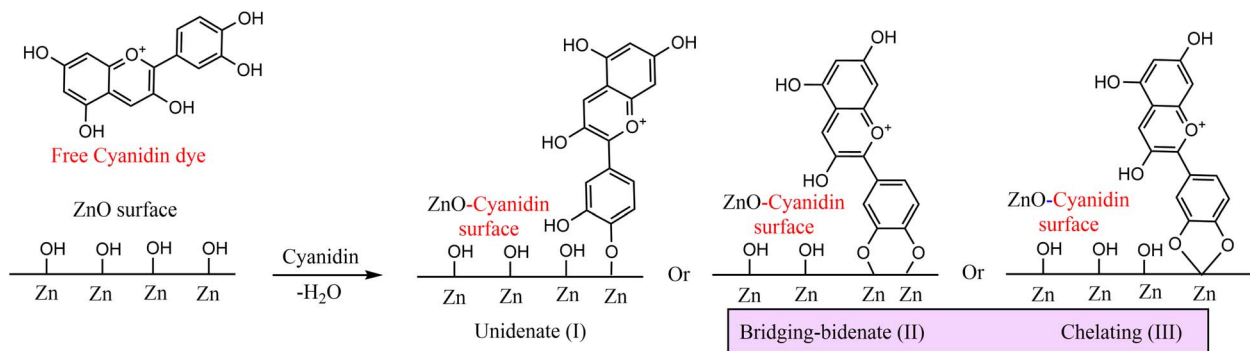
Fig. 1 Potential approaches for complexation between ZnONPs and cyanidin (Cy) dye are being explored.
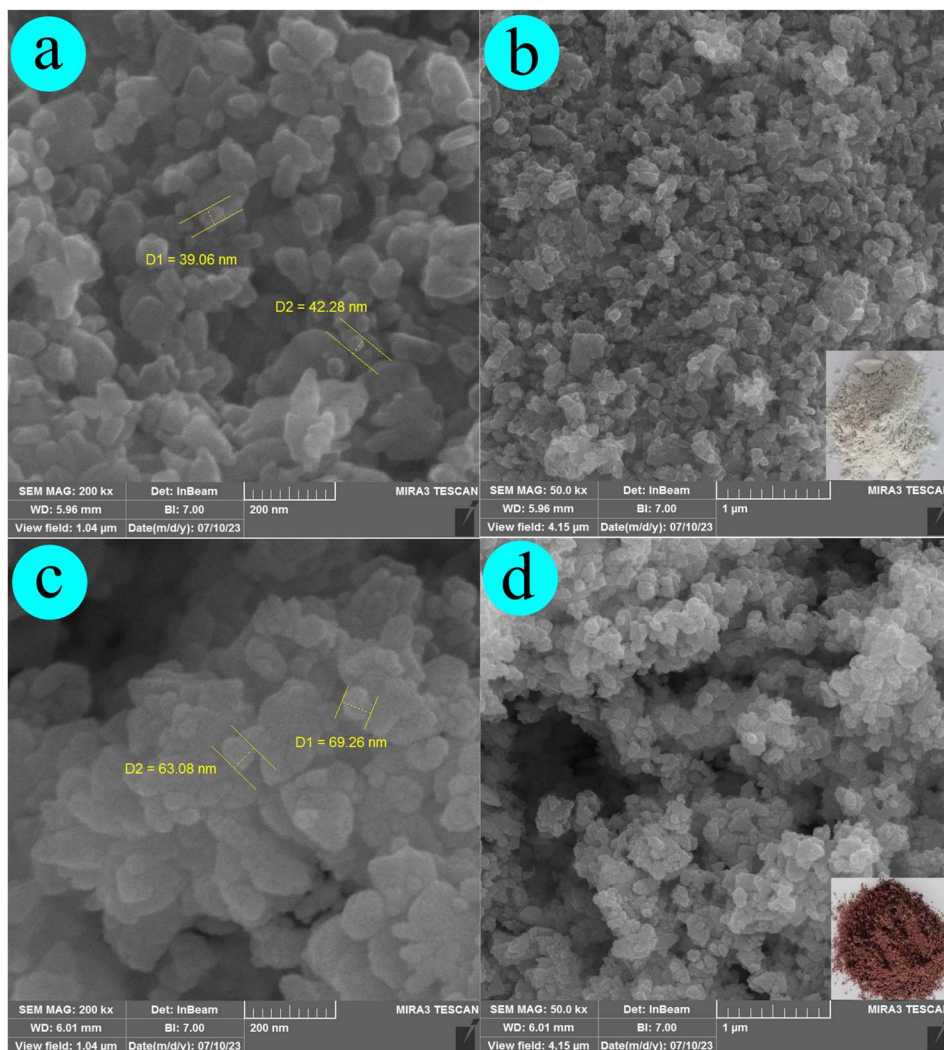
Fig. 2 SEM images of (a and b) Ag-ZnONPs, and (c and d) Ag-ZnONPs@Cy in different magnifications.

the distribution of particle sizes remains mostly uniform. Furthermore, Fig. 3a displays the EDX spectrum of the Ag-ZnONPs, accompanied by a quantitative determination of the constituent elements. The spectrum and mapping images collectively indicate the absence of impurities in the synthesized Ag-ZnONPs, affirming their successful formation.

Fig. 2c, d, and 3b depict the SEM, EDX, and elemental mapping results of the composite material Ag-ZnONPs@Cy.
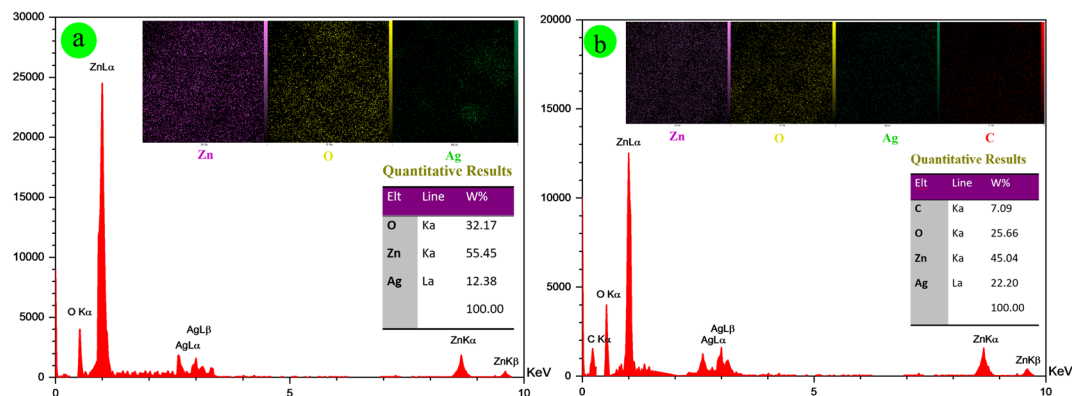
Fig. 3 EDX spectrum and elemental mapping of (a) Ag-ZnONPs, and (b) Ag-ZnONPs@Cy.

Compared with Ag-ZnONPs, an observable growth in particle size (ranging from 60 to 80 nm) is apparent; however, the fundamental shape and morphology remain consistent. The elemental composition analysis reveals the presence of Zn (45.04 W%), O (25.66 W%), Ag (22.20 W%), and C (7.09 W%) elements in Ag-ZnONPs@Cy, confirming the successful synthesis of the composite without any undesirable impurities. These findings are in alignment with those obtained through the X-ray diffraction (XRD) technique.

3.3.2. Vibrational spectroscopy study. FT-IR spectroscopy was employed to identify the functional groups in cyanidin dye, Ag-ZnO, and Ag-ZnO@Cy. The most prominent peaks are highlighted in Fig. 4. Cyanidin dye exhibited several characteristic peaks that were in good agreement with previously reported work on anthocyanin dye extracted from blueberry powder.[46]

In the spectra of all three compounds, an intense broad peak appeared around 3400 cm^{-1}, attributed to OH stretching vibrations. Additionally, vibrational C–H stretching was observed near 3000 cm^{-1}, C=C stretching was present at 2109 cm^{-1}, and conjugated alkene vibrations were found at 1615 cm^{-1}. Moreover, C–O–C stretching was observed at 1105 cm^{-1} in both Cy and Ag-ZnO@Cy spectra but was absent in Ag-ZnO. An interesting observation was an intense band in the 500–600 cm^{-1} range, which served as a characteristic peak for Zn–O stretching in both Ag-ZnO and Ag-ZnO@Cy, but was not present in the cyanidin dye spectrum. These results strongly suggest that cyanidin dye was successfully conjugated with Ag-ZnONPs, as indicated by the presence of specific peaks in Ag-ZnO@Cy that were absent in Ag-ZnO and cyanidin dye spectra.

3.3.3. XRD study. X-Ray diffraction has been utilized for elucidating the arrangement of crystalline solids and determining the phase composition of the synthesized Ag-ZnONPs@Cy, as illustrated in Fig. 5. The XRD pattern of the composite reveals distinct sets of ZnO, Ag, and Cy characteristics. The observed peaks, accompanied by their corresponding
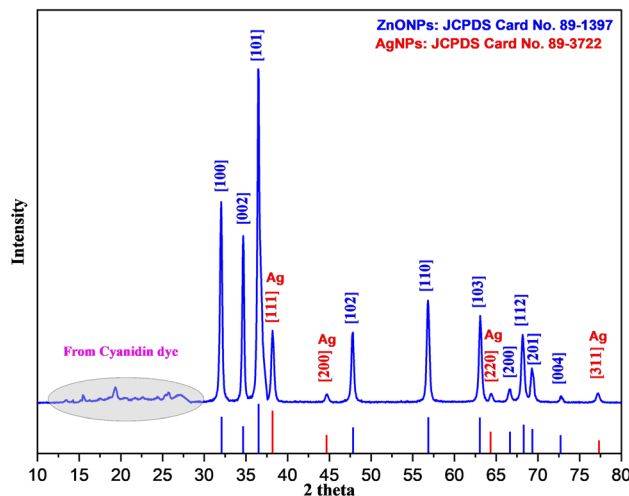

Fig. 5 XRD spectra of Ag-ZnONPs@Cy shows the peaks of each ZnONPs, AgNPs and cyanidin dye.

indices, namely 32.13° (100), 34.62° (002), 36.54° (101), 47.71° (102), 56.57° (110), 63.14° (103), 66.54° (200), 67.80° (112), 69.17° (201), and 72.81° (004), confirm the hexagonal structure of ZnONPs within the ternary nanocomposite. This structural arrangement aligns precisely with the established reference data (JCPDS, card no. 89-1397).[47] Furthermore, the peaks situated at 38.09° (111), 44.2° (200), 64.62° (220), and 77.16° (311) validate the face-centered cubic configuration of the silver nanoparticles, consistent with the data found in (JCPDS, card no. 89-3722).[48] In addition, some faint peaks are discernible in the 2 theta range of 15°–30°, indicative of cyanidin dye within the ternary nanocomposite. These outcomes corroborate findings from other studies wherein organic components were linked with nanoparticles.[49,50] The XRD analysis outcomes collectively affirm the successful synthesis of the Ag-ZnONPs@Cy ternary composite. The average crystalline size of the Ag-ZnONPs@Cy nanocomposites is determined by applying Scherrer's equation ($D = k\lambda/\beta \cos\theta$). Here, D signifies the crystal size, with k representing the crystal shape constant set at 0.90, λ denoting the X-ray wavelength at 0.15406 nm, β indicating the full width at half maximum (FWHM), and θ corresponding to the diffraction angle. The application of this equation yields an average crystallite size of 27.42 nm for the ternary composite.

3.3.4. UV-vis and DRS study. Upon exposure to light, electrons within the cyanidin dye can be energized, transitioning from their highest occupied molecular orbital (HOMO) to the lowest unoccupied molecular orbital (LUMO). This process empowers the dye to transfer electrons to the connected metal oxide nanoparticles. This intrinsic property renders the natural dye valuable as a photosensitizer in solar cell applications.[51] Numerous investigations have been conducted regarding its UV-Vis absorption characteristics and energy band gap, both in theoretical and practical contexts, using various solvents such as water, acetonitrile, and ethanol. The computed range for wavelength lies between approximately 300 nm to 700 nm, and the associated band gap energy is estimated to be within the
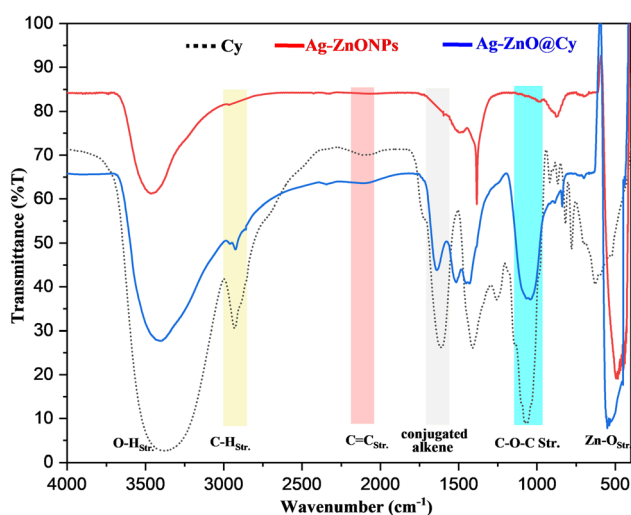

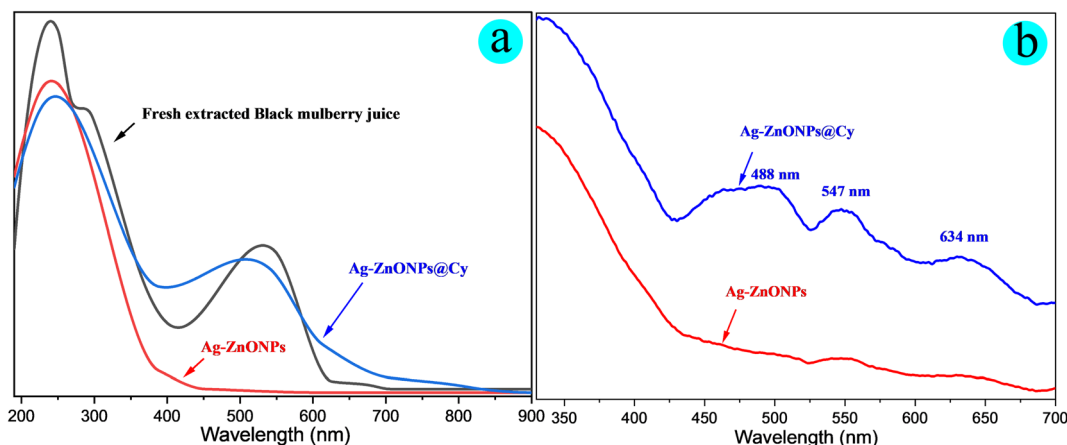Fig. 4 FT-IR spectra for cyanidin dye (black dots), Ag-ZnO (red), and Ag-ZnO@Cy (blue).

Fig. 6 (a) UV-Vis spectra of fresh extracted black mulberry juice, Ag-ZnONPs and Ag-ZnONPs@Cy, and (b) DRS spectra of Ag-ZnONPs and Ag-ZnONPs@Cy.

range of 2.1 to 2.81 eV.[51–54] In light of the outcomes documented in existing literature, it is reasonable to anticipate that the cyanidin dye can serve effectively as a sensitizer for activating metal oxides with broadband gap energies within the visible light spectrum.

In this study, the optical properties of the fabricated catalysts, unmodified Ag-ZnONPs and Ag-ZnONPs@Cy, were investigated using UV-visible spectroscopy and diffuse reflection spectroscopy (UV-vis DRS) in both liquid and solid states. The obtained results, depicted in Fig. 6, clearly demonstrated that Ag-ZnONPs lacked effective absorption of visible light. In contrast, Ag-ZnO@Cy exhibited a substantial extension of its visible light-harvesting range, attributed to the broad overlap of the dye (Cy) with the visible light spectrum (350–650 nm). This enhanced visible light absorption confirmed the successful combination of ZnONPs with the dye (Cy) in Ag-ZnO@Cy. Due to its ability to efficiently harness visible light, Ag-ZnO@Cy presents itself as a promising candidate for catalyzing organic transformations under green conditions with different visible light sources.

3.4. Photocatalytic activity

The powders of Ag-ZnONPs and Ag-ZnONPs@Cy exhibited colors of white and reddish-brown, respectively, as shown in Fig. S1 of the ESI.† The UV-vis and diffuse reflectance spectra (DRS) of Ag-ZnONPs and Ag-ZnONPs@Cy are depicted in Fig. 6a and b. In Fig. 6a, the UV-vis spectroscopy of the synthesized

catalyst, both before and after being coupled with the cyanidin dye, is explained. Ag-ZnONPs@Cy displayed wide absorption bands in the visible light range (350–650 nm), with a peak absorption wavelength of around 495 nm. On the other hand, unmodified Ag-ZnONPs showed no significant absorption activity. It is worth noting that the λ_{max} (peak absorption wavelength) of Ag-ZnONPs@Cy was shifted towards the blue region compared to the free cyanidin (Cy) dye. The solid-phase diffuse reflectance spectroscopy (DRS) analysis of the catalysts is illustrated in Fig. 6b. Interestingly, the modified Ag-ZnONPs exhibited a λ_{max} at 488 nm, and two additional peaks were observed at 547 nm and 634 nm. In contrast, the unmodified Ag-ZnONPs displayed a weak absorption peak. This phenomenon can be attributed to the surface plasmon resonance (SPR) of silver (Ag) nanoparticles or atom clusters located on the surface of the metal oxides, as described by previous studies.[55,56]

Initially, the photocatalytic performance of Cy, Ag-ZnONPs, and Ag-ZnONPs@Cy in catalyzing the reduction of nitrobenzene to produce aniline under visible light irradiation ($\lambda > 425$ nm) was examined. The reaction conditions for converting nitrobenzene to aniline are outlined in Scheme 2. When Cy dye was used alone, no products were detected. In contrast, employing the Ag-ZnONPs catalyst resulted in an isolated yield of 18% in the presence of TEOA after 30 minutes. Notably, in the case of Ag-ZnONPs@Cy, an impressive yield of 98% was achieved.

The efficiency of photocatalysis for both catalysts was assessed in the context of reducing nitrobenzene (NB) to generate aniline (AN) using acetonitrile as the solvent. Upon initiating the reaction, the maximum absorption of NB was noted at a wavelength of 270 nm. The UV-vis spectra illustrating the photo-reduction process of NB to AN were provided in Fig. 7a and b for Ag-ZnONPs and Ag-ZnONPs@Cy, respectively.

As the reaction commenced, a new peak emerged at 230 nm, corresponding to aniline formation, while the intensity of the 270 nm peak diminished. This reduction in intensity indicates the conversion of NB to AN, aligning with findings reported in prior investigations.[57,58]
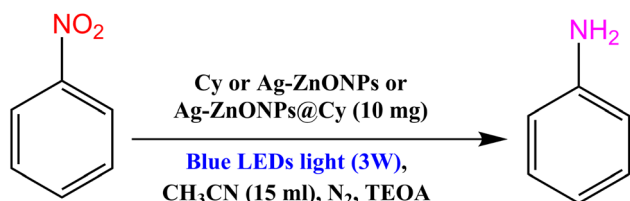
Scheme 2 Photocatalytic reduction of nitrobenzene to aniline under optimized conditions.
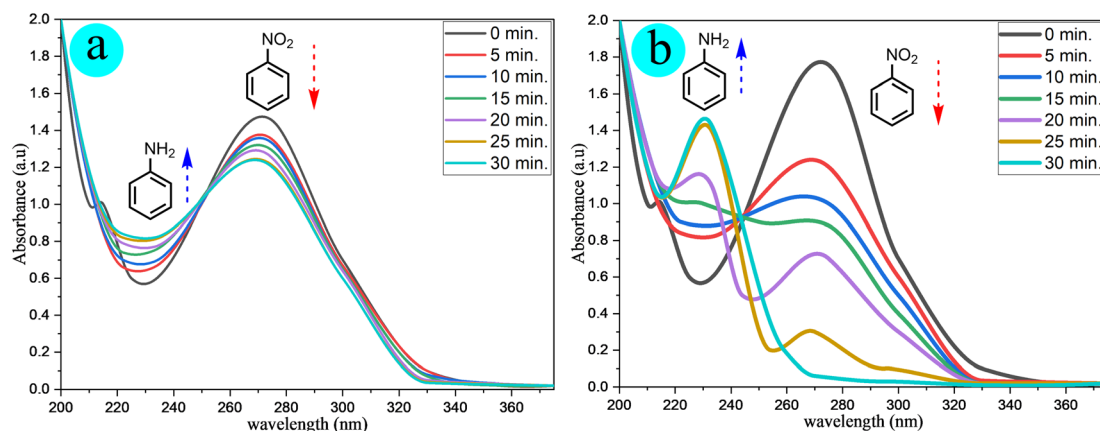
Fig. 7 UV-visible spectra obtained after 30 minutes for the transformation of NB to AN using (a) Ag-ZnONPs and (b) Ag-ZnONPs@Cy.

Drawing from the results of the conversion analysis, it can be inferred that the integration of the cyanidin dye significantly amplifies the photocatalytic effectiveness of Ag-ZnONPs. Consequently, throughout this study, Ag-ZnONPs@Cy was employed for hydrogenating aromatic nitro compounds into their corresponding amino compounds.

Several control experiments were also performed to determine the optimum condition before using the catalyst for

hydrogenation of nitrobenzene derivatives which is summarized in Table 1, which includes performing the reaction in the dark, testing different LED light sources, solvent effect, amount of catalyst loading for the conversion, sacrificial electron donor (TEOA), the presence of O_2 as electron trapper.

Observations were made indicating that the reaction does not proceed in the absence of light (Table 1, entry 5). Conversely, using blue LED light leads to a higher yield percentage (Table 1, entry 3) compared to the outcomes with white, green, and red LEDs (Table 1, entries 1, 2, and 4). Various solvents, including ethanol, acetonitrile, DMSO, ethyl acetate, and water, were tested, and CH_3CN emerged as the optimal solvent, providing a superior yield percentage (Table 1, entry 3). Notably, using 10 mg of the loaded catalyst yielded improved results (Table 1, entry 3). The multifunctional character of TEOA has been demonstrated in previous studies,[58,59] serving as an electron donor to the dye sensitizer to restore the oxidized form to its original state and also acting as a proton source for hydrogenation of nitroarenes to aminoarenes.[60,61] The absence of TEOA led to the non-formation of the product in the reaction (Table 1, entry 17). Similarly, conducting the reaction in the presence of atmospheric O_2 instead of N_2 did not yield the desired product (Table 1, entry 16).

Utilizing the optimal conditions (Table 1, entry 3) for the reduction of nitroarenes to aminoarenes (as shown in Table 2), the desired products were obtained successfully, achieving remarkable percentage yields. These initial outcomes from the developed ternary composite (Ag-ZnONPs@Cy) for efficient hydrogenation provide strong motivation for further explorations in the realm of photoredox catalysis, encompassing a diverse array of organic transformations.

Table 1 The optimization and control experiments of the catalysis system for the reduction of NB to AN[a]

Entry	Light source	Cat. (X mg)	Solvent	Yield (%)
1	White LEDs-3W	10	CH_3CN	42
2	Green LEDs-3W	10	CH_3CN	74
3	**Blue LEDs-3W**	**10**	**CH_3CN**	**98**
4	Red LEDs-3W	10	CH_3CN	19
5	Dark	10	CH_3CN	0
6	Blue LEDs-3W	—	CH_3CN	2
7	Blue LEDs-3W	2	CH_3CN	25
8	Blue LEDs-3W	3	CH_3CN	48
9	Blue LEDs-3W	5	CH_3CN	83
10	Blue LEDs-3W	10	CH_3CN	98
11	Blue LEDs-3W	15	CH_3CN	72
12	Blue LEDs-3W	10	H_2O	Trace
13	Blue LEDs-3W	10	EtOH	31
14	Blue LEDs-3W	10	DMSO	51
15	Blue LEDs-3W	10	EtOAc	56
16[b]	Blue LEDs-3W	10	CH_3CN	29
17[c]	Blue LEDs-3W	10	CH_3CN	0
18[d]	Blue LEDs-3W	10	CH_3CN	98

[a] Standard condition: NB (1 mmol, 1 equiv.), CH_3CN (15 mL), TEOA (10 equiv.) blue LEDs (3 W, $\lambda > 425$ nm) under N_2 and the reaction vessel was sealed. The reaction was carried out at room temperature in 30 min reaction time. [b] The reaction performed in air. [c] The reaction was conducted without TEOA. [d] The reaction time was 2 h.

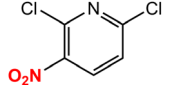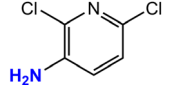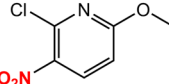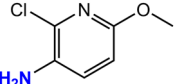### 3.5. Regeneration and reusability of the catalyst
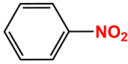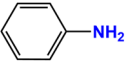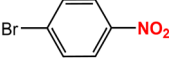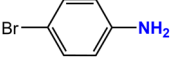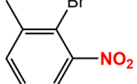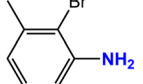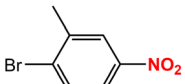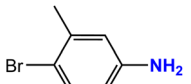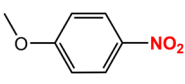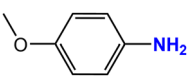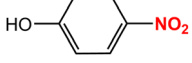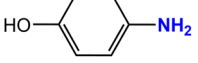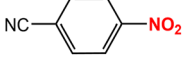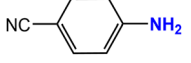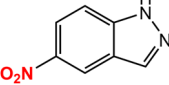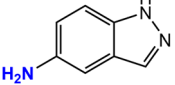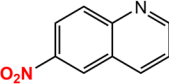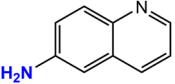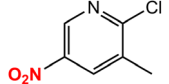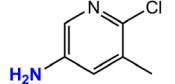
The practical application of photocatalysts heavily relies on their reusability, making it a pivotal aspect to investigate. In this context, the recyclability of Ag-ZnONPs@Cy was examined through a series of six recycling experiments involving NB reduction. After each reduction process, the photocatalyst was

Table 2 The range of substrates explored using the newly developed Ag–ZnONPs@Cy photocatalyst[a]

Entry	Substrate	Product	Time (min)	Isolated yield (%)
1			30	98
2			40	96
3			55	89
4			45	93
5			75	95
6			35	91
7			25	97
8			60	90
9			85	98
10			65	94
11			50	82
12			55	85

[a] The reaction condition: nitroarene (1 mmol, 1 equiv.), TEOA (10 equiv.), catalyst (10 mg), solvent; CH_3CN (15 mL), N_2 gas, blue LEDs light (3 W, λ > 425 nm) and room temperature.

retrieved through centrifugation, followed by washing, drying, and subsequent utilization in the succeeding cycle.

Fig. 8a and b depict the IR spectrum and XRD patterns of the ternary catalyst, both before initial use and after undergoing six usage cycles. It is evident that there are no significant alterations in the structure of the catalyst. This observation serves as a confirmation of the exceptional stability over prolonged usage periods. Fig. 8c displays the progressive photo reduction of NB to AN by Ag-ZnONPs@Cy across six successive cycles. Notably, there is no discernible decline in the photocatalytic efficiency, with only a marginal 2.5% decrease in efficacy. These results

validate the remarkable and consistent photocatalytic stability of Ag-ZnONPs@Cy over multiple cycles, alongside its exceptional performance.

3.6. Mechanistic study

Utilizing findings from UV-vis and DRS investigations, along with insights from comprehensive literature reviews,[51–54] it is evident that the cyanidin dye exhibits a band-gap energy situated within the visible light spectrum, as depicted in Fig. 6a and b. This characteristic renders the dye proficient in absorbing photonic energy, converting it into electronic energy.
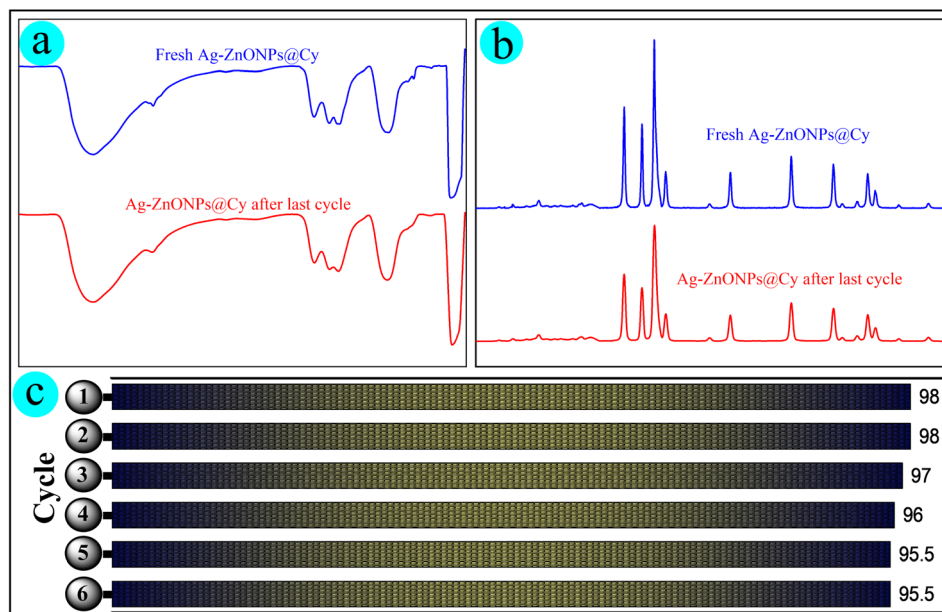
Fig. 8 Representation of (a) infrared spectra, (b) X-ray diffraction patterns, and (c) the reusability of Ag-ZnONPs@Cy after six cycles, recovering at the end of each reduction cycle.

Furthermore, in the context of a photo-redox catalysis system, the cyanidin dye demonstrates the ultrafast capability to inject electrons into the associated metal oxides, thereby facilitating efficient electron transfer.[62]

To uncover the inherent reaction mechanism, the utilization of 1,4-benzoquinone served as a means to determine if the process adheres to a radical pathway. Notably, benzoquinone is recognized for its capability to quench superoxide radicals.[63] Despite this, it was noted that the introduction of benzoquinone had no impact on the reaction rate. Consequently, it is reasonable to deduce that the reaction mechanism does not rely on a radical pathway.

Based on the findings derived from this study, along with a comprehensive review of the literature,[40,59,61,64,65] as well as

quenching and control experiments, we have formulated a mechanistic proposal for the conversion of nitroarenes to aminoarenes utilizing cyanidin dye-sensitized Ag-ZnONPs. The sequence is outlined as follows: upon exposure to blue light, the cyanidin dye transitions from its ground state (Cy) to an excited state (Cy*). In this excited state, the dye molecule injects electrons into the conduction band of ZnONPs. Subsequently, these electrons are transferred to the surface of Ag, leading to the generation of H_2 by extracting a proton from the sacrificial donor (TEOA), thereby facilitating the reduction process. The catalytic cycle concludes as the sacrificial donor reduces the excited dye back to its initial state (Cy), thus completing the cycle. A comprehensive depiction of this process can be found in Fig. 9.
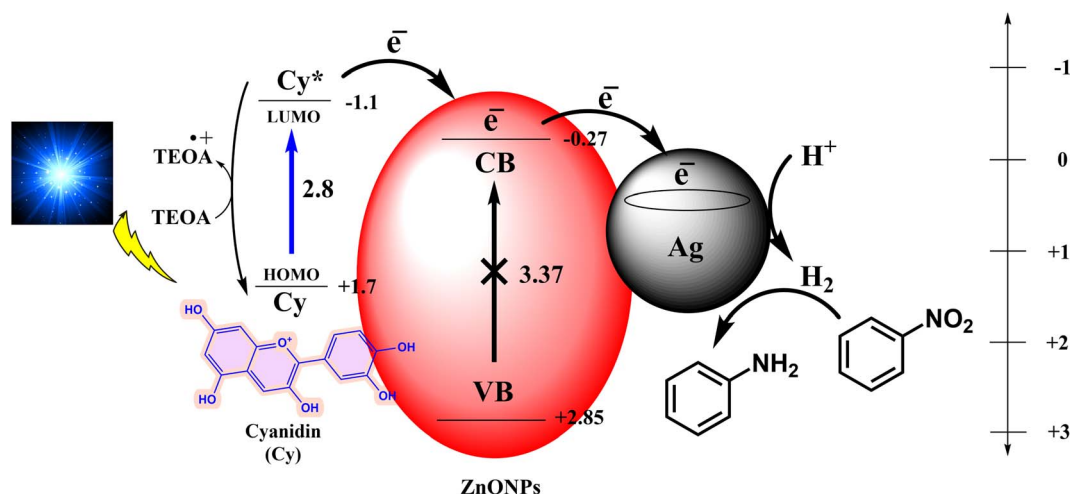

Fig. 9 A proposed mechanism for the reduction of nitroarenes to aminoarenes by Ag-ZnONPs@Cy.

4. Conclusion

This study presents the successful modification of Ag-doped ZnONPs into a visible-light-active hybrid photocatalyst by integrating them with the cyanidin (Cy) dye sensitizer. The resulting ternary material (Ag-ZnONPs@Cy) was synthesized using a multistep, straightforward, and environmentally conscious green method. Various characterization techniques such as FT-IR, XRD, SEM, elemental mapping, EDX, UV-Vis, and DRS were employed to ascertain the identity and photocatalytic efficacy of the produced ternary composite. Subsequently, this composite was employed as a photocatalyst to reduce aromatic nitro compounds into their corresponding amines under blue light irradiation. Impressively, the reaction demonstrated remarkably short completion times (25–85 minutes) along with good to excellent isolated yield percentages. Introducing a sacrificial electron donor (TEOA) facilitated electron and proton mediation within the reaction. A series of control experiments were conducted to elucidate the mechanistic pathway, revealing that the reaction proceeded through an electron transfer route. Given the pivotal importance of recovery and reusability in heterogeneous photocatalysts, the regeneration and reusability of the fabricated catalyst were explored. The results indicated that the catalyst maintained excellent photocatalytic activity for at least six cycles upon regeneration. Overall, the outcomes from this study underscore the potential of the ternary composite Ag-ZnONPs@Cy as a promising photocatalyst for diverse organic transformations under visible light exposure. This approach offers a straightforward, cost-effective, and environmentally friendly avenue for achieving these transformations.

Conflicts of interest

The author declares no conflict of interest.

References

1 Z. Long, Q. Li, T. Wei, G. Zhang and Z. Ren, *J. Hazard. Mater.*, 2020, **395**, 122599.

2 M. Kokkonen, P. Talebi, J. Zhou, S. Asgari, S. A. Soomro, F. Elsehrawy, J. Halme, S. Ahmad, A. Hagfeldt and S. G. Hashmi, *J. Mater. Chem. A*, 2021, **9**, 10527–10545.

3 D. A. Kader, S. O. Rashid and K. M. Omer, *RSC Adv.*, 2023, **13**, 9963–9977.

4 J. J. Samuel and F. K. Yam, *Mater. Res. Express*, 2020, **7**, 015051.

5 P. Riente and T. Noël, *Catal. Sci. Technol.*, 2019, **9**, 5186–5232.

6 D. A. Kader and S. Omer, *Mol. Catal.*, 2023, **547**, 113409.

7 P. V. Govardhana Reddy, B. Rajendra Prasad Reddy, M. Venkata Krishna Reddy, K. Raghava Reddy, N. P. Shetti, T. A. Saleh and T. M. Aminabhavi, *J. Environ. Manage.*, 2021, **279**, 111603.

8 C. Anushree, D. Nanda Gopala Krishna and J. Philip, *J. Mol. Liq.*, 2021, **337**, 116429.

9 H. Dabhane, S. Ghotekar, P. Tambade, S. Pansambal, R. Oza and V. Medhane, *Eurasian J. Chem.*, 2021, **12**, 86–108.

10 M. Nasrollahzadeh, Z. Nezafat, M. G. Gorab and M. Sajjadi, *Mol. Catal.*, 2020, **484**, 110758.

11 P. Chen, Z. Guo, X. Liu, H. Lv, Y. Che, R. Bai, Y. Chi and H. Xing, *J. Mater. Chem. A*, 2019, **7**, 27074–27080.

12 Y. Rangraz, F. Nemati and A. Elhampour, *Appl. Surf. Sci.*, 2020, **507**, 145164.

13 K. Kombaiah, J. J. Vijaya, L. J. Kennedy, K. Kaviyarasu, R. J. Ramalingam and H. A. Al-Lohedan, *J. Nanosci. Nanotechnol.*, 2018, **19**, 2590–2598.

14 R. Akbari, *J. Mater. Sci.: Mater. Electron.*, 2021, **32**, 15801–15813.

15 V. Cittrarasu, D. Kaliannan, K. Dharman, V. Maluventhen, M. Easwaran, W. C. Liu, B. Balasubramanian and M. Arumugam, *Sci. Rep.*, 2021, **11**, 1–15.

16 S. Pan, T. B. Goudoulas, J. Jeevanandam, K. X. Tan, S. Chowdhury and M. K. Danquah, *Front. Bioeng. Biotechnol.*, 2021, **9**, 1–9.

17 N. Maity, N. Bruchiel-Spanier, O. Sharabani-Yosef, D. Mandler and N. Eliaz, *Mater. Adv.*, 2023, **4**, 3026–3036.

18 P. Mahadevi and S. Sumathi, *Results Chem.*, 2023, **6**, 101026.

19 A. A. Mohamed, A. Fouda, M. A. Abdel-Rahman, S. E. D. Hassan, M. S. El-Gamal, S. S. Salem and T. I. Shaheen, *Biocatal. Agric. Biotechnol.*, 2019, **19**, 101103.

20 M. Carofiglio, S. Barui, V. Cauda and M. Laurenti, *Appl. Sci.*, 2020, **10**, 5194.

21 R. Aboorvakani, S. J. Kennady Vethanathan and K. U. Madhu, *J. Alloys Compd.*, 2020, **834**, 155078.

22 Q. A. Drmosh, I. Olanrewaju Alade, M. Qamar and S. Akbar, *Chem. – Asian J.*, 2021, **16**, 1519–1538.

23 R. Liu, Y. Chen, S. Ding, Y. Li and Y. Tian, *Sol. Energy Mater. Sol. Cells*, 2019, **203**, 110161.

24 A. M. Chandran, S. Varun, S. C. Karumuthil, S. Varghese and P. K. S. Mural, *ACS Appl. Nano Mater.*, 2021, **4**, 1798–1809.

25 M. Goswami, *Opt. Mater.*, 2020, **109**, 110400.

26 T. Varadavenkatesan, E. Lyubchik, S. Pai, A. Pugazhendhi, R. Vinayagam and R. Selvaraj, *J. Photochem. Photobiol., B*, 2019, **199**, 111621.

27 K. Singh, Neha, M. Kumar, H. Singh and G. Singh, *Mater. Today: Proc.*, 2023, DOI: 10.1016/j.matpr.2023.03.002.

28 I. Kohli, R. Zubair, A. B. Lyons, A. F. Nahhas, T. L. Braunberger, M. Mokhtari, E. Ruvolo, H. W. Lim and I. H. Hamzavi, *Photochem. Photobiol.*, 2019, **95**, 1285–1287.

29 K. R. Reddy, M. Hassan and V. G. Gomes, *Appl. Catal., A*, 2015, **489**, 1–16.

30 A. Dhakshinamoorthy, Z. Li and H. Garcia, *Chem. Soc. Rev.*, 2018, **47**, 8134–8172.

31 X. Yu and S. M. Cohen, *J. Am. Chem. Soc.*, 2016, **138**, 12320–12323.

32 X. Lang, J. Zhao and X. Chen, *Angew. Chem., Int. Ed.*, 2016, **55**, 4697–4700.

33 M. Hosseini-Sarvari, M. Koohgard, S. Firoozi, A. Mohajeri and H. Tavakolian, *New J. Chem.*, 2018, **42**, 6880–6888.

34 C. Xu, P. Ravi Anusuyadevi, C. Aymonier, R. Luque and S. Marre, *Chem. Soc. Rev.*, 2019, **48**, 3868–3902.

35 J. Luo, S. Zhang, M. Sun, L. Yang, S. Luo and J. C. Crittenden, *ACS Nano*, 2019, **13**, 9811–9840.

36 A. Truppi, F. Petronella, T. Placido, M. Striccoli, A. Agostiano, M. L. Curri and R. Comparelli, *Catalysts*, 2017, **7**, 100.

37 G. Zhang, G. Kim and W. Choi, *Energy Environ. Sci.*, 2014, **7**, 954–966.

38 N. Zhou, V. López-Puente, Q. Wang, L. Polavarapu, I. Pastoriza-Santos and Q. H. Xu, *RSC Adv.*, 2015, **5**, 29076–29097.

39 R. Medhi, M. D. Marquez and T. R. Lee, *ACS Appl. Nano Mater.*, 2020, **3**, 6156–6185.

40 S. Bhar and R. Ananthakrishnan, *RSC Adv.*, 2015, **5**, 20704–20711.

41 S. Slathia, T. Gupta and R. P. Chauhan, *Phys. B*, 2021, **621**, 413287.

42 H. Nishikiori, D. Natori, H. Ebara, K. Teshima and T. Fujii, *J. Photochem. Photobiol., A*, 2016, **327**, 51–57.

43 M. Ben Manaa, N. Issaoui, Y. O. Al-Ghamdi, H. Belmabrouk and A. Ben Lamine, *RSC Adv.*, 2020, **10**, 27615–27632.

44 H. Shahroosvand, P. Abbasi, M. Ameri and M. Riahi, *Int. J. Photoenergy*, 2011, **2011**, 1–10.

45 T. Kamegawa, H. Seto, S. Matsuura and H. Yamashita, *ACS Appl. Mater. Interfaces*, 2012, **4**, 6635–6639.

46 S. Jeyaram and T. Geethakrishnan, *Results Opt.*, 2020, **1**, 100010.

47 E. Shah, P. Mahapatra, A. V. Bedekar and H. P. Soni, *RSC Adv.*, 2015, **5**, 26291–26300.

48 P. K. Khanna, N. Singh, D. Kulkarni, S. Deshmukh, S. Charan and P. V. Adhyapak, *Mater. Lett.*, 2007, **61**, 3366–3370.

49 R. Aladpoosh and M. Montazer, *Carbohydr. Polym.*, 2015, **126**, 122–129.

50 T. Tchouank Tekou Carol, A. Srivastava, J. Mohammed, S. Sharma, G. Mukhtar and A. K. Srivastava, *SN Appl. Sci.*, 2020, **2**, 1–8.

51 M. Bužančić Milosavljević, A. Mravak, M. Perić Bakulić and V. Bonačić-Koutecký, *RSC Adv.*, 2023, **13**, 6010–6016.

52 K. Galappaththi, A. Lim, P. Ekanayake and M. I. Petra, *Int. J. Photoenergy*, 2017, **2017**, 1–6.

53 P. Ekanayake, M. R. R. Kooh, N. T. R. N. Kumara, A. Lim, M. I. Petra, V. N. Yoong and L. C. Ming, *Chem. Phys. Lett.*, 2013, **585**, 121–127.

54 K. Galappaththi, P. Ekanayake and M. I. Petra, *Sol. Energy*, 2018, **161**, 83–89.

55 I. Ahmad, E. Ahmed and M. Ahmad, *SN Appl. Sci.*, 2019, **1**, 1–12.

56 W. Liu, D. Chen, S. H. Yoo and S. O. Cho, *Nanotechnology*, 2013, **24**, 405706.

57 J. Zhang, T. Yao, H. Zhang, X. Zhang and J. Wu, *Nanoscale*, 2016, **8**, 18693–18702.

58 T. Akhtar, H. Nasir, E. Sitara, S. A. B. Bukhari and J. W. Schwank, *Surf. Interfaces*, 2023, **39**, 102997.

59 S. Füldner, T. Mitkina, T. Trottmann, A. Frimberger, M. Gruber and B. König, *Photochem. Photobiol. Sci.*, 2011, **10**, 623–625.

60 A. C. Tsipis and A. A. Sarantou, *Dalton Trans.*, 2021, **50**, 14797–14809.

61 S. Füldner, R. Mild, H. I. Siegmund, J. A. Schroeder, M. Gruber and B. König, *Green Chem.*, 2010, **12**, 400–440.

62 N. J. Cherepy, G. P. Smestad, M. Gra and J. Z. Zhang, *J. Phys. Chem. B*, 1997, **5647**, 9342–9351.

63 O. Fónagy, E. Szabó-Bárdos and O. Horváth, *J. Photochem. Photobiol., A*, 2021, **407**, 113057.

64 S. Kohtani, S. Nishioka, E. Yoshioka and H. Miyabe, *Catal. Commun.*, 2014, **43**, 61–65.

65 S. Kohtani, M. Mori, E. Yoshioka and H. Miyabe, *Catalysts*, 2015, **5**, 1417–1424.